Published Online: 29 January, 2018 | Supp Info: http://doi.org/10.1084/jem.20170901

JEM

Deficiency in T follicular regulatory cells promotes autoimmunity

Weiwei Fu,[1] Xindong Liu,[2] Xiang Lin,[3] Han Feng,[1] Lin Sun,[1] Shuran Li,[4] Hairong Chen,[4] Hong Tang,[5] Liwei Lu,[3] Wei Jin,[1] and Chen Dong[1]

[1]Institute for Immunology and School of Medicine, Tsinghua University, Beijing, China
[2]Institute of Pathology and Southwest Cancer Center, Southwest Hospital, Third Military Medical University, Chongqing, China
[3]Department of Pathology and Shenzhen Institute of Research and Innovation, University of Hong Kong, Hong Kong, China
[4]CAS Key Laboratory of Infection and Immunity, Institute of Biophysics and [5]CAS Key Laboratory of Molecular Virology and Immunology, Institute Pasteur of Shanghai, Chinese Academy of Sciences, Beijing, China

T follicular regulatory (Tfr) cells are a new subset of regulatory T (T reg) cells localized in the germinal center to limit the humoral response. Until now, the physiological function of Tfr cells has been largely unknown. In this study, we developed a *Bcl6*$^{fl/fl}$*Foxp3Cre* mouse to analyze the function of Tfr cells in immune and autoimmune responses. These mice exhibited enhanced immunity to influenza virus; moreover, *Bcl6*$^{fl/fl}$*Foxp3Cre/Cre* mice developed late-onset spontaneous autoimmune diseases, affecting the salivary glands with lymphocyte infiltration and antibody deposition. In a mouse experimental Sjögren's syndrome model, ablation of *Bcl6* in T reg cells greatly enhanced disease development. Conversely, *Bcl6*$^{fl/fl}$*Cd4Cre* mice were protected in the model. Thus, our study indicates that Tfr cells control autoimmune diseases and can be targeted in infectious and autoimmune disease.

Journal of Experimental Medicine

INTRODUCTION

T follicular helper (Tfh) cells, a subset of CD4$^+$ T cells characterized by Bcl6 expression (Johnston et al., 2009; Nurieva et al., 2009; Yu et al., 2009), provide essential help to B cells during germinal center (GC) reactions through CD40 and the cytokines IL-21 and IL-4 (Reinhardt et al., 2009; Zotos et al., 2010; Crotty, 2011; Lüthje et al., 2012). Tfh cells drive B cells to undergo Ig class switching and somatic hypermutation (Victora et al., 2012) and facilitate high-affinity B cell selection via death receptor CD95 on B cells (Takahashi et al., 2001). B cells within GCs can also differentiate into memory B cells or long-lived plasma cells (Victora et al., 2010). Thus, precise control of GC reactions is critical to ensure production of high-affinity antibodies that do not react to self-antigens (Vinuesa et al., 2009).

T follicular regulatory (Tfr) cells offer negative regulation on GC responses. Similar to Tfh cells, Tfr cells express CXCR5, ICOS, and PD-1, as well as the transcription factor Bcl6 (Chung et al., 2011; Linterman et al., 2011; Wollenberg et al., 2011). However, Tfr cells coexpress typical T regulatory (T reg) cell markers, such as Foxp3, GITR, Blimp-1, and CTLA-4. Tfr cells are specific for the immunized antigen, irrespective of self or foreign (Aloulou et al., 2016). Tfr cell differentiation is primed by dendritic cells (Gerner et al., 2015) at an early stage and further matured by B cells (Kerfoot et al., 2011; Linterman et al., 2011; Sage et al., 2014a). Costimulatory signals CD28 and ICOS (Linterman et al., 2011; Sage et al., 2013) and transcription factor Bcl-6 (Chung et al., 2011; Linterman et al., 2011) are important for Tfr generation. Id2 and Id3 limit Tfr cell formation (Miyazaki et al., 2014), whereas NFAT facilitates CXCR5 up-regulation in Foxp3$^+$ T cells (Vaeth et al., 2014). Cytokine IL-21 inhibited Tfr cell proliferation through Bcl-6 suppression of IL-2 responsiveness (Sage et al., 2016; Jandl et al., 2017). Tfr cells were shown to control the magnitude of GC response after immunization through CTLA-4 (Sage et al., 2014b; Wing et al., 2014). However, the physiological and pathological roles of Tfr cells are largely unknown.

Here, we analyzed *Bcl6*$^{fl/fl}$*Foxp3Cre* (KO) mice, which have decreased CXCR5$^+$PD1$^+$CD4$^+$Foxp3$^+$ Tfr cells, in infection and autoimmune diseases. KO mice exhibited enhanced protection to influenza virus. More importantly, *Bcl6*$^{fl/fl}$*Foxp3Cre/Cre* mice were more prone to develop autoimmune diseases and more susceptible to an experimental Sjögren's syndrome (ESS) model. Therefore, Tfr cells are crucial controls for autoimmune diseases.

RESULTS AND DISCUSSION

Generation and analysis of *Bcl6*$^{fl/fl}$*Foxp3Cre/Cre* mice

To study Tfr cells, we specifically deleted the *Bcl6* gene in Foxp3$^+$ T reg cells (*Bcl6*$^{fl/fl}$*Foxp3Cre* KO mice). First, we immunized KO mice and *Bcl6*$^{fl/fl}$*Foxp3WT/WT* (WT) mice with 4-hydroxy-3-nitrophenyl (NP)–conjugated KLH or KLH in CFA. CXCR5$^+$PD1$^+$ cells were observed in the T

Correspondence to Chen Dong: chendong@tsinghua.edu.cn

The Rockefeller University Press
J. Exp. Med. 2018 Vol. 215 No. 3 815–825
https://doi.org/10.1084/jem.20170901

reg ($CD4^+Foxp3^+$) cell population in the draining lymph nodes (dLNs) of WT mice on day 4 after immunization (Fig. S1 A). In contrast, both percentages (left) and cell numbers (right) of Tfr cells were strongly diminished in KO mice (Fig. S1 A). Moreover, the immunofluorescence analysis of dLNs at day 9 after immunization revealed that, compared with WT mice, KO mice had barely detectable $Foxp3^+$ cells in the PNA^+ GC region (Fig. S1 B). Thus, deletion of *Bcl6* in T reg cells reduced Tfr cells, and although CXCR5 and PD-1 were still found in some T reg cells in KO mice, T reg cell localization in GC was impaired.

To assess whether Tfr cell deficiency affects GC reactions, we analyzed Tfh and GC B cells in KO mice after immunization. The percentages of Tfh cells were modestly increased in KO mice, but their cell numbers were not changed (Fig. S1 C). Although GC B cells were not changed (Fig. S1 D), the light zone (LZ)/dark zone (DZ) ratio was significantly increased (Fig. S1 E). Tfr deficiency did not affect Th1, Th2, or Th17 cells in dLNs (unpublished data). KO mice produced significantly higher levels of NP29-specific IgG2a, IgG2c, and IgA but lower levels of IgG1, with comparable levels of IgG2b, IgG3, and IgM, than WT mice (Fig. S1 F). However, antibody affinity maturation, as measured by the ratio of NP4/NP29, had no obvious change (unpublished data).

We also immunized mice with NP-KLH in CFA and administered boosters of NP-KLH in IFA 30 d after primary immunization. Before and on day 3 after the secondary challenge, we observed a significantly increased $CD19^+GL7^-Fas^-IgD^-CD38^+$ memory B cell population (Wang et al., 2017; Fig. S1, H and I). Furthermore, KO mice showed significant increases in NP4/NP29 ratios of IgG or IgG2a, indicating greater affinity (Fig. S1 G).

Deletion of *Bcl6* in $Foxp3^+$ T reg cells results in Tfr cell defects, which consequentially augments GC B cell responses with greater LZ in the primary reaction, and the memory B cell differentiation and antibody affinity maturation in the secondary response.

Tfr deficiency enhances influenza virus protection

We further addressed the functional role of Tfr cells in influenza virus infection. After intranasal injection with influenza virus A/Puerto Rico/8 (PR8, H1N1), Tfr KO mice displayed no obvious weight reduction compared with WT mice from day 3 to day 9 (Fig. 1 A). At day 9 after infection, the viral hemagglutinin (HA) mRNA expression from lungs of control mice was >14-fold higher than those in KO mice (Fig. 1 B). This difference was further confirmed using littermate $Bcl6^{fl/wt}$ *Foxp3Cre/Cre* mice as control (Fig. S1, J and K). Although the Tfr cell population after infection was small, the percentages but not the numbers of Tfr cells were significantly diminished in KO mice (Fig. 1 C). However, $CXCR5^+Bcl6^+$ Tfh cells and Fas^+GL7^+ GC B cells in lung dLNs (Fig. 1, D and E), or in lung and spleen (not depicted), had no obvious change in percentages or total cell numbers in KO mice. Although Tfr deficiency did not affect Th1, Th2, or Th17 cells in lung dLNs (Fig. 1 F), IFN-γ expression in $CD4^+Foxp3^-Bcl6^+$ Tfh cells was significantly increased (Fig. 1G). IFN-γ was reported to induce class switching to complement-activating isotypes, such as IgG2 (Snapper and Paul, 1987). Interestingly, although total antiviral IgG was unchanged, IgG2c production was increased in the KO mice (Fig. 1 H).

Defects in Tfr cells cause humoral autoimmunity

KO mice 6–8 wk old were healthy and fertile, with Tfh and GC B cell populations comparable to those of WT mice (Fig. S2, A–D). Only splenic $CD4^+$ T cells producing IFN-γ and IL-4 were modestly increased (Fig. S2, E–G). At this age, anti–double-stranded DNA (dsDNA) IgG was not increased in the sera of KO mice (Fig. S2 H). However, KO mice at 12 wk showed increased numbers of Tfh cells (Fig. S2 J) and GC B cells (Fig. S2 K) in the spleen, peripheral lymph nodes (pLNs), and mesenteric lymph nodes (MLNs). Although sera anti-dsDNA (Fig. S2 L) did not change statistically, some KO mice began to increase production, with subtle IgG deposition (Fig. S2 M). KO mice at 30 wk showed significant inflammatory cell infiltrations in some organs, including lung and pancreas, especially in the salivary gland (SG; Fig. 2 A), whereas kidney, intestine, liver, and heart were not affected (not depicted). This phenotype was further verified using littermate $Bcl6^{fl/fl}$*Foxp3Cre/WT* mice as controls (Fig. S2 Q). Moreover, KO mice produced higher concentrations of anti-dsDNA, anti-ANA, anti-SG, and anti–nuclear ribonucleoprotein (nRNP)/Sm antibodies in their sera (Fig. 2 C and Fig. S2, N–P). Also, analyses of SG and kidney revealed considerable IgG deposition in KO mice (Fig. 2 B). Interestingly, the saliva flow rate, reflecting the function of SGs, was significantly reduced in KO mice (Fig. 2 D). When we analyzed Tfr cells, we found they were increased in the spleen and pLNs but not MLNs in 30-wk-old mice compared with younger ones (Fig. 2 E). Moreover, the percentages and numbers of Tfr cells were significantly diminished in the spleen and pLNs of KO mice (Fig. 2 E). However, only the percentages but not numbers were reduced in MLNs, possibly because of increased cell numbers in MLNs in KO mice (Fig. 2 E). Because excessive numbers of Tfh cells have recently been associated with autoimmune diseases in both mice and humans (Gómez-Martín et al., 2011; Crotty, 2014), we assessed Tfh cells in aged $Bcl6^{fl/fl}$*Foxp3Cre/Cre* mice. As expected, enhanced production of Tfh cells was observed in the spleen, pLN, and MLN of KO mice compared with WT mice (Fig. 2 F). Consistently, we observed spontaneous accumulation of $GL7^+Fas^+$ GC B cells in pLN and MLN of KO mice (Fig. 2 G). The results were confirmed using the littermate $Bcl6^{fl/fl}$*Foxp3Cre/WT* mice as controls (Fig. S2, R and S). However, IFN-γ, IL-4, and IL-17A production in the $CD4^+$ T cells had no obvious change (Fig. 2, H–J), suggesting that defects in Tfr cells only selectively affected GC reactions. Tfr deficiency thus causes spontaneous GC formation and humoral autoimmunity in mice, associated with uncontrolled Tfh and GC B cell differentiation.

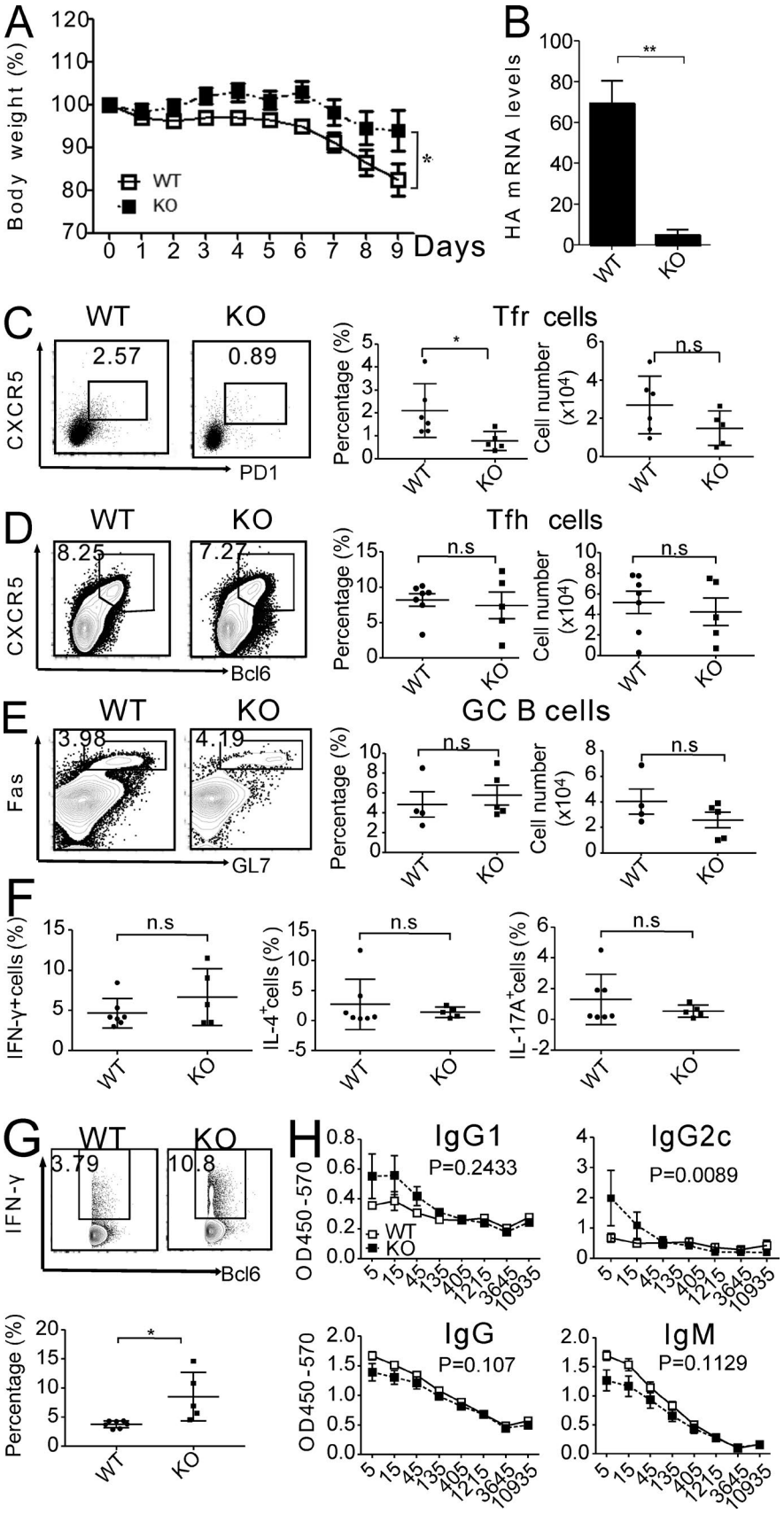

Figure 1. **Loss of Bcl6 in T reg cells enhances protection to influenza virus infection. (A)** Body weights of control and KO mice were monitored daily after infection. $n = 5$ or 7 per group. **(B)** Mice were sacrificed at day 9 after infection, and viral titers in the lungs were assessed by quantitative RT-PCR measurement of active HA gene expression. $n = 4$. **(C)** FACS staining (left), frequency quantitation (middle), and cell number (right) analysis of $CXCR5^+Bcl6^+$ Tfr cells in $CD4^{+-}$ $Foxp3^+$ cells in lung dLN from influenza-infected control and KO mice. $n = 5$–6 per group. **(D and E)** FACS staining (left), frequency quantitation (middle), and cell number (right) analysis of $CXCR5^+Bcl6^+$ Tfh cells in $CD4^+Foxp3^-$ cells (D) and $GL\text{-}7^+Fas^+$ GC B cells in $B220^+$ cells (E) in lung dLNs from infected control and KO mice. $n = 5$ or 7 per group in D; 4 or 5 per group in E. **(F and G)** After restimulation with PMA and ionomycin for 5 h, IFN-γ, IL-4, and IL-17A expression in $CD4^+$ T cells (F) and FACS staining (top row) and frequency quantitation (bottom row) of IFN-γ^+ cells in $CD4^+Foxp3^-Bcl6^+$ cells (G) in lung dLNs from the influenza-infected control and KO mice were measured by flow cytometric analysis. $n = 5$–7 per group. **(H)** At day 9 after infection, sera levels of Ig specific for virus were measured by ELISA. $n = 4$–7 per group. *Bcl6$^{fl/fl}$Foxp3Cre/Cre* mice were KO, and *Bcl6$^{fl/fl}$Foxp3WT/WT* mice from the *Bcl6$^{fl/fl}$Foxp3Cre/WT*x*Bcl6$^{fl/fl}$Foxp3WT* breeder were used as control. All data are representative of two independent experiments. Data shown are mean ± SEM; two-tailed *t* test; p-values in A and G were analyzed by two-way ANOVA. *, $P < 0.05$; **, $P < 0.01$; ***, $P < 0.001$; n.s., no significance.

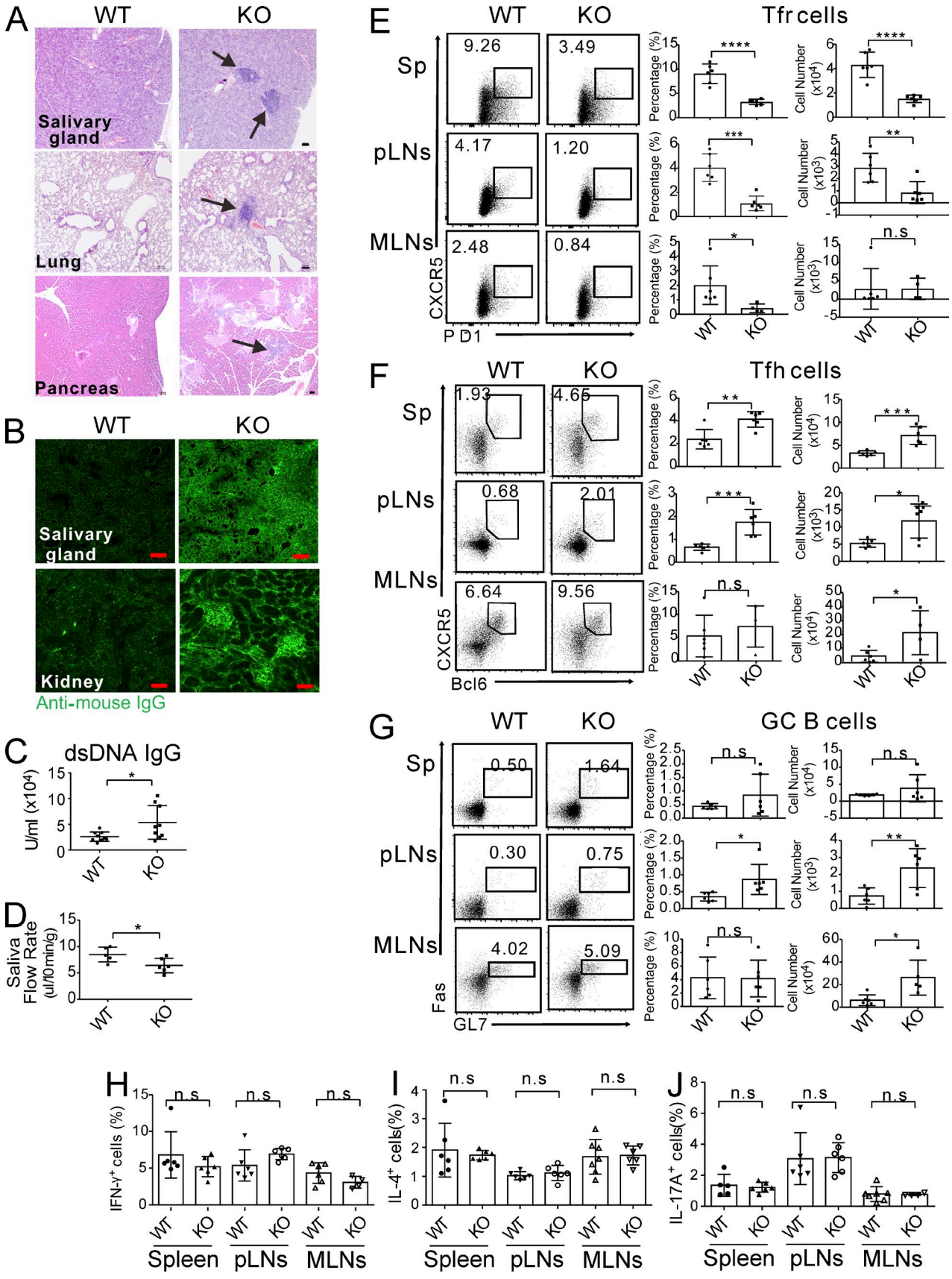
A
WT
KO
Salivary gland
Lung
Pancreas
B
WT
KO
Salivary gland
Kidney
Anti-mouse IgG
C
dsDNA IgG
U/ml (x10⁴)
WT
KO
D
Saliva Flow Rate (ul/10min/g)
WT
KO
E
WT
KO
Tfr cells
Sp
pLNs
MLNs
9.26
3.49
4.17
1.20
2.48
0.84
CXCR5
PD1
Percentage (%)
Cell Number (x10⁴)
Cell Number (x10³)
n.s
F
WT
KO
Tfh cells
Sp
pLNs
MLNs
1.93
4.65
0.68
2.01
6.64
9.56
CXCR5
Bcl6
G
WT
KO
GC B cells
Sp
pLNs
MLNs
0.50
1.64
0.30
0.75
4.02
5.09
Fas
GL7
H
IFN-γ⁺ cells (%)
n.s
WT
KO
Spleen
pLNs
MLNs
I
IL-4⁺ cells(%)
n.s
J
IL-17A⁺ cells(%)
n.s

Tfr deficiency enhances ESS development

Because decreased salivary flow rate, increased anti-ANA and anti-SG antibodies, and massive inflammatory cell infiltration and deposition of IgG in the SG are key diagnostic criteria for Sjögren's syndrome (SS), we hypothesized that Tfr deficiency promotes the development of SS. Thus, we set up the ESS model as reported (Lin et al., 2015), in which experimental mice exhibited reduced saliva secretion (Fig. S3 A), elevated serum autoantibody production (Fig. S3 B), and tissue destruction associated with lymphocytic infiltration in submandibular gland (Fig. S3 C). Further analysis revealed significantly increased frequencies and numbers of Tfh cells (Fig. S3 D), Tfr cells (Fig. S3 E), and GC B cells (Fig. S3 F) in the cervical lymph nodes (CLNs) compared with control mice immunized with adjuvant.

Remarkably, immunized KO mice exhibited further reduced saliva flow rates 6 wk after immunization (Fig. 3 A), as well as elevated SG-specific antibodies (Fig. 3 B). Moreover, tissue destruction (Fig. 3, C and D) and IgG deposition were enhanced in the SG of KO mice 15 wk after immunization (Fig. 3 E). We conducted pathological analysis on the SG 5 wk after immunization and found that KO, but not WT, mice began to have infiltrated lymphocytes in the SG (Fig. 3 F), which was confirmed using littermate *Bcl6*$^{fl/fl}$*Foxp3Cre/WT* mice as controls (Fig. S3 G). WT and KO mice thus had differences in disease initiation 5 wk after induction. Flow cytometric (left) and cell number (right) analysis revealed reduced Tfr cells in CLNs of KO mice, whereas WT mice showed obvious Tfr response upon ESS induction (Fig. 3 G). Furthermore, although the Tfh population did not significantly change (Fig. 3 H), GC B cell percentages but not numbers were increased in the CLN of KO mice (Fig. 3 I). However, Th1 and Th17 or serum IFN-γ and IL-17A levels were not greatly affected (Fig. 3, J–M). Tfr cells therefore play a critical protective role in ESS development by controlling the GC and antibody response.

Tfh cells play a critical role in the development of ESS

To further verify whether GC and Tfh response plays an important role in ESS development, we used *Bcl6*$^{fl/fl}$*Cd4*^{Cre} mice (Liu et al., 2016). When *Bcl6*$^{fl/fl}$*Cd4*^{Cre} mice were subjected to the ESS model, we found the saliva flow to be partially but not significantly recovered compared with the WT mice (Fig. 4 A). Moreover, SG-specific antibody production was significantly diminished in KO mice (Fig. 4 B). Remarkably, *Bcl6*$^{fl/fl}$*Cd4*^{Cre} mice exhibited no histological change or IgG deposition in SG up to 15 wk after immunization (Fig. 4, C–E). As expected, flow cytometric analysis showed very minimal Tfh and GC B cells in the CLN (Fig. 4, F and G). Further analysis of the Th cell subsets showed that Th1 cells were somewhat decreased but not significantly (Fig. 4 H), whereas Th17 cells were down-regulated (Fig. 4 I), with serum IL-17A production (Fig. 4 K) also decreased. Tfh cells thus play a critical role in the development of ESS.

Interestingly, saliva flow rates in the ESS model were not greatly affected in the absence of Tfh or Tfr cells; thus, the Tfh/Tfr axis might not contribute greatly to the saliva flow rate change. There may be compensatory mechanisms driving saliva flow rate reduction.

Previous studies, including in vivo adoptive transfer experiments and in vitro suppression assays, have demonstrated the inhibitory function of Tfr cells in GC response (Chung et al., 2011; Sage et al., 2013, 2014a,b, 2015). In this study, we used a *Bcl6*$^{fl/fl}$*Foxp3Cre/Cre* mouse to analyze the roles of Tfr cells under physiological and pathological conditions. Our data showed that unlike the general T reg cell–deficient mice, *Bcl6*$^{fl/fl}$*Foxp3Cre/Cre* mice were largely healthy at young ages and did not exhibit greatly altered primary immune response to immunized antigen. However, defects in Tfr cells enhanced the secondary humoral response to immunized antigens and promoted immunity to influenza virus, suggesting that Tfr may function to limit immunity to persistent antigens or infection.

Bcl6 was reported to inhibit the expression of T-bet and GATA3 as well as the function of RORγt (Nurieva et al., 2009), and *Bcl6*$^{-/-}$ T reg cells showed increased *Rorc* but reduced *Tbx21* expression (Chung et al., 2011). Therefore, we measured Th1, Th2, and Th17 cells in all experiments. Tfr deficiency did not alter the numbers of Th1, Th2, or Th17 cells in the dLN or immune organs at steady state. However, IFN-γ production by Tfh cells was significantly increased in KO mice, which indicates that Tfr cells could selectively control the antigen-specific Tfh response.

Until now, whether Tfr cells regulate the pathogenesis of autoimmune diseases has been unknown. In our study, *Bcl6*$^{fl/fl}$*Foxp3Cre/Cre* mice developed late-onset systemic

Figure 2. **Loss of Bcl6 in T reg cells leads to humoral autoimmunity. (A)** Histopathology analysis of SG, lung, and pancreas from WT and KO mice at 30 wk of age. Black arrows indicate the immune cell infiltrates in KO mice. Bars, 100 µm. *n* = 6 per group. **(B)** Anti-IgG immunofluorescent staining of SG and kidney. WT, *n* = 3; KO, *n* = 6 per group. Bars, 50 µm. **(C)** Anti-dsDNA autoantibodies in the sera of WT and KO mice were measured by ELISA. *n* = 9 per group. **(D)** Saliva flow rates were measured in WT and KO mice. *n* = 5–6 per group. **(E)** FACS staining (left), frequency quantitation (middle), and cell number (right) analysis of CXCR5$^+$Bcl6$^+$ Tfr cells in CD4$^+$Foxp3$^+$ cells in different organs from the old steady-state control and KO mice. *n* = 6 per group. **(F)** FACS staining (left), frequency quantification (middle), and cell number (right) analysis of Bcl6$^+$CXCR5$^+$ Tfh cells in CD4$^+$Foxp3$^-$ T cells from different organs of WT and KO mice. **(G)** FACS staining (left), frequency quantification (middle), and cell number (right) analysis of GL7$^+$Fas$^+$ GC B cells in B220$^+$ cells from different organs of WT and KO mice. **(H–J)** After restimulation with PMA and ionomycin for 5 h, IFN-γ (H), IL-4 (I), and IL-17A (J) expression in CD4$^+$ T cells from different organs was measured by flow cytometric analysis. All mice were 30-wk-old unmanipulated mice. *n* = 6 per group in F–J. SP, spleen. All experimental data were verified in at least two independent experiments. *Bcl6*$^{fl/fl}$*Foxp3Cre/Cre* mice were KO, and *Bcl6*$^{fl/fl}$*Foxp3WT/WT* mice from the *Bcl6*$^{fl/fl}$*Foxp3Cre/WTxBcl6*$^{fl/fl}$*Foxp3WT* breeder were used as control. Data shown are mean ± SEM; two-tailed *t* test; *, P < 0.05; **, P < 0.01; ***, P < 0.001; n.s., no significance.

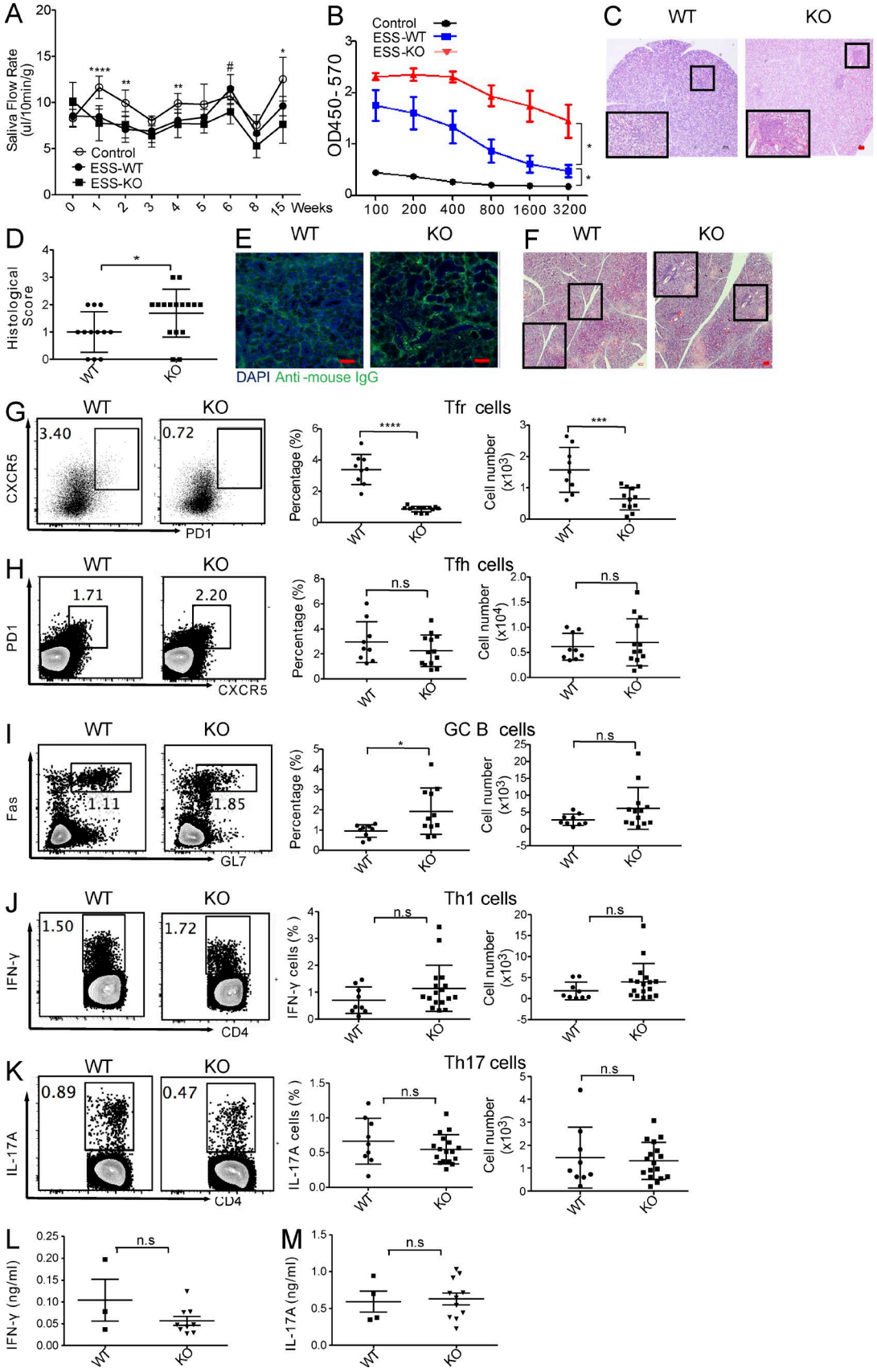
A
Saliva Flow Rate (ul/10min/g)
Control
ESS-WT
ESS-KO
Weeks
B
Control
ESS-WT
ESS-KO
OD450 - 570
C
WT
KO
D
Histological Score
E
WT
KO
DAPI Anti -mouse IgG
F
WT
KO
G
WT
KO
3.40
0.72
CXCR5
PD1
Tfr cells
Percentage (%)
Cell number (x10³)
H
WT
KO
1.71
2.20
PD1
CXCR5
Tfh cells
Percentage (%)
Cell number (x10⁴)
n.s
I
WT
KO
1.11
1.85
Fas
GL7
GC B cells
Percentage (%)
Cell number (x10³)
J
WT
KO
1.50
1.72
IFN-γ
CD4
Th1 cells
IFN-γ cells (%)
Cell number (x10³)
K
WT
KO
0.89
0.47
IL-17A
CD4
Th17 cells
IL-17A cells (%)
Cell number (x10³)
L
IFN-γ (ng/ml)
M
IL-17A (ng/ml)

autoimmune diseases, including SS. These results prompted us to test Tfr KO mice in an animal model for SS. Indeed, we found that Tfr deficiency greatly enhanced ESS development. Interestingly, we found that Tfh and GC B cell responses, but not Th1 or Th17 responses, were selectively affected by Tfr deficiency. We thus analyzed *Bcl6*$^{fl/fl}$*Cd4*^{Cre} mice and found them to be resistant to ESS induction. These data firmly demonstrate the roles of Tfh/Tfr in ESS.

Recently, Botta et al. (2017) and Wing et al. (2017) reported that Tfr cells contain CD25$^-$ and CD25$^+$ subpopulations in influenza infection and immunization models. CD25$^-$ Tfr cells, mostly localized in the GCs and acting as the primary suppressive cells in established GCs, could be inhibited by high levels of IL-2 during the immune response. CD25$^+$ Tfr cells, a precursor population mostly localized in the T cell zone, may be involved in regulation of the earlier stages of B cell responses. RNA sequencing data showed that CD25$^-$ Tfr cells had higher expression of Tfh-related molecules, such as Bcl6, whereas CD25$^+$ Tfr cells were significantly enriched for general T reg genes. These results are consistent with our hypothesis of stepwise development of Tfh cells, in which Bcl6 is highly up-regulated in mature Tfh cells (Liu et al., 2012). In our immunization and influenza infection models, which resemble early immune responses, most Tfr cells might be CD25$^+$. So the Tfr deficiency mainly affected the cytokine production of Tfh cells, with minimal effect to the GC response. According to Botta et al. (2017), some T reg cells down-regulated CD25, up-regulated Bcl-6, and differentiated into Tfr cells once the immune response was resolved, then migrated into the B cell follicles to prevent the expansion of self-reactive B cell clones. Our immunofluorescence results demonstrate significant defects of Foxp3$^+$ cells in the GC from mice with *Bcl6* deletion in T reg cells, suggesting a stronger effect to the function of CD25$^-$ Tfr cells. Consistently, we detected higher autoantibody production and GC response in the old *Bcl6*$^{fl/fl}$*Foxp3Cre/Cre* mice and in the ESS model. We also found GC responses to be not always the same in different organs at steady state, maybe because of different proportions of CD25$^-$ Tfr cells in different lymphoid organs. This variation may result from the availability of STAT5 signaling, because a lower proportion of T reg cells are pSTAT5$^+$ in the spleen than in the LNs (Liu et al., 2015). Thus, because of different levels and characteristics of Tfr cells in different immune reactions and time points, and even in various immune organs, defects in Tfr cells lead to distinct outcomes in B cell response. But consistently in all experiments, Tfr cells appear to control antigen-specific antibody response, especially that against self-antigens.

Altogether, our current work demonstrates the physiological and pathological roles of Tfr cells in several models and supports a critical role of Tfh/Tfr cells in antibody-mediated autoimmunity. Targeting this axis may serve as a novel strategy for autoimmune diseases such as SS.

MATERIALS AND METHODS

Mice

The *Bcl6*$^{fl/fl}$ mice were generated previously (Liu et al., 2016). *Bcl6*$^{fl/fl}$ mice (B6 × 129 N1 background) were crossed with *Cd4*^{Cre} (C57BL/6 background) mice for one generation to generate *Bcl6*$^{fl/fl}$*Cd4*^{Cre} mice. *Foxp3YFP-Cre* mice were provided by A. Rudensky (Memorial Sloan Kettering Cancer Center, New York, NY). The *Foxp3Cre* mice (C57BL/6 background) were crossed with *Bcl6*$^{fl/fl}$ mice to generate *Bcl6*$^{fl/fl}$*Foxp3Cre/Cre* mice. Thus, the experimental mice were on the N2 background. *Bcl6*$^{fl/fl}$*Foxp3WT/WT* mice from *Bcl6*$^{fl/fl}$*Foxp3Cre/WT*x*Bcl6*$^{fl/fl}$*Foxp3WT* breeders were generally used as controls. The phenotypes in various experiments have been confirmed using littermate *Bcl6*$^{fl/wt}$*Foxp3Cre/Cre* or *Bcl6*$^{fl/fl}$*Foxp3Cre/WT* mice as controls. All the mice used in this study were female. Experimental mice were age-matched and housed under specific pathogen–free conditions in the animal facility of Tsinghua University. All animal protocols were approved by governmental and Tsinghua guidelines for animal welfare.

Immunization and flow cytometry

6–8-wk-old mice were immunized with NP-KLH (1 mg/ml) emulsified in CFA (1 mg/ml) s.c. For secondary re-

Figure 3. **Ablation of *Bcl6* in T reg cells enhances ESS development. (A)** ESS model was set up and analyzed after 15 wk. The kinetics of the saliva flow rates were measured during the 15 wk after SG protein immunization (ESS) in both WT and KO mice and adjuvant immunization (control). *n* = 5–10 per group. *, statistics analysis between control and ESS-WT group; #, analysis between ESS-WT and ESS-KO group. **(B)** IgG autoantibodies against SG antigens were detected in the serum samples from ESS mice and controls 15 wk after first immunization by ELISA. *n* = 4–5 per group. **(C)** Histological evaluation of glandular destruction in WT and KO mice after ESS induction was performed on tissue sections of submandibular glands with H&E staining. Bars, 100 µm. **(D)** Infiltrated lymphocytes in the SGs were assessed for histological scores. WT, *n* = 12; KO, *n* = 16. **(E)** Anti-IgG immunofluorescent staining of SGs. WT, *n* = 4; KO, *n* = 6. Bars, 50 µm. **(F)** Histological evaluation of glandular destruction in WT and KO mice at 5 wk after ESS induction was performed on tissue sections of submandibular glands with H&E staining. Bars, 100 µm. *n* = 5 per group. **(G–I)** FACS staining (left), frequency quantification (middle), and cell number (right) analysis of CXCR5$^+$PD1$^+$ Tfr cells in CD4$^+$Foxp3$^+$ cells (G), CXCR5$^+$PD1$^+$ Tfh cells in CD4$^+$Foxp3$^-$ cells (H), and Fas$^+$GL7$^+$ GCB in B220$^+$ cells (I) in CLNs of WT and KO mice at 15 wk after first immunization. *n* = 9 or 13. **(J and K)** After restimulation with PMA and ionomycin for 5 h, FACS staining (left), frequencies (middle), and cell number (right) analysis of IFN-γ and IL-17-producing Th1 (J) and Th17 cells (K) among CD4$^+$ T cells in CLN of WT and KO mice was performed by flow cytometry. *n* = 9 or 17 in J and K. **(L and M)** Serum IFN-γ (L) and IL-17 (M) levels were detected by ELISA. WT, *n* = 3 or 4; KO, *n* = 9 or 11. Data in G–K were pooled from two independent experiments. All experimental data were verified in at least two independent experiments. *Bcl6*$^{fl/fl}$*Foxp3Cre/Cre* mice were KO, and *Bcl6*$^{fl/fl}$*Foxp3WT/WT* mice from the *Bcl6*$^{fl/fl}$*Foxp3Cre/WT*x*Bcl6*$^{fl/fl}$*Foxp3WT* breeder were used as control. Data shown are mean ± SEM; two-tailed *t* test; p-values in B were analyzed by two-way ANOVA; * or #, P < 0.05; **, P < 0.01; ***, P < 0.001; n.s., no significance.

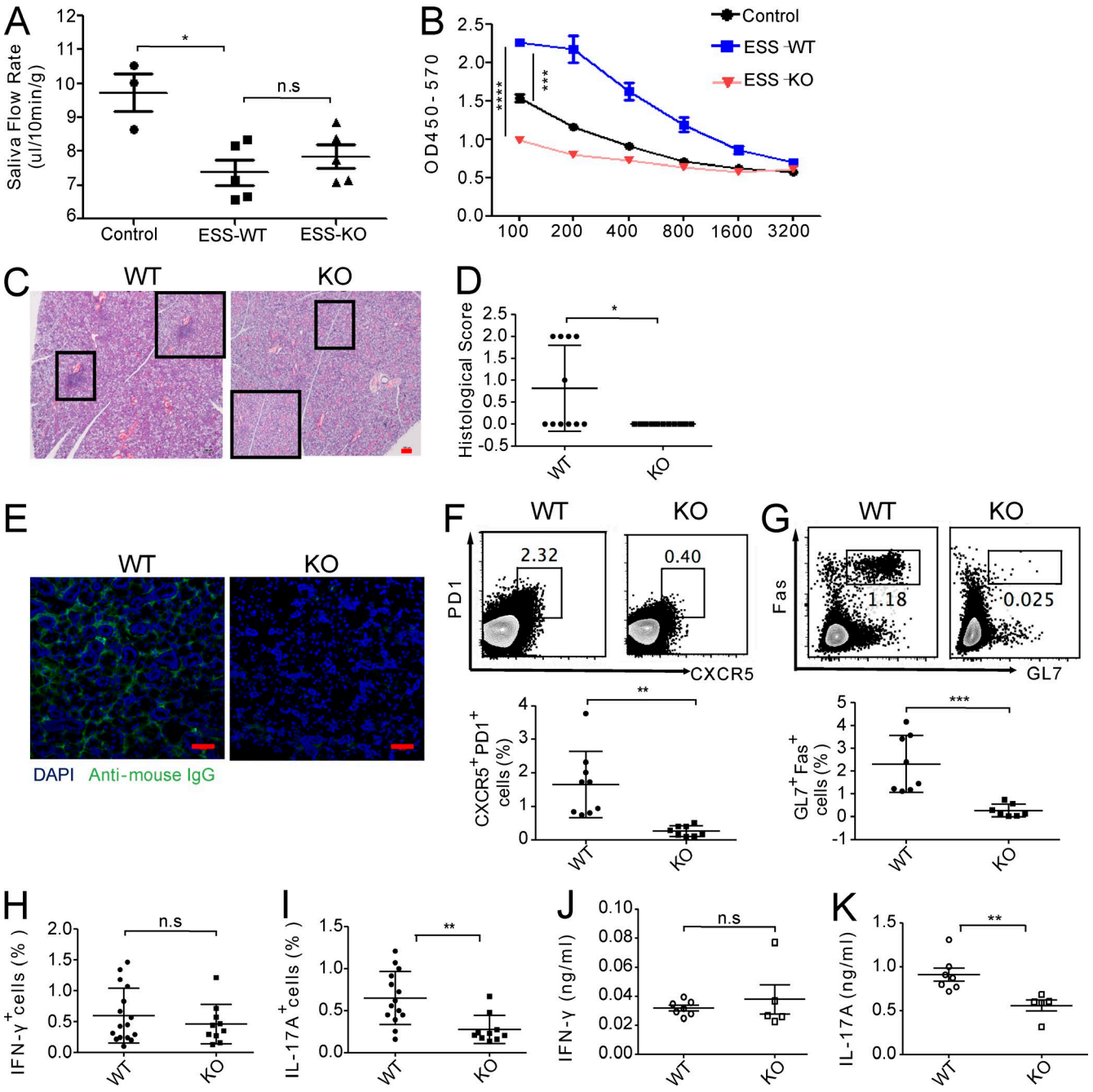

Figure 4. **GC response plays a critical role in the development of ESS. (A)** Saliva flow rates were measured 15 wk after SG protein-immunization (ESS) in both WT and KO mice and adjuvant immunization (control). *n* = 3 or 5. **(B)** Autoantibodies against SG antigens were detected in the serum samples from ESS WT and KO mice and controls 15 wk after first immunization by ELISA. *n* = 3 or 5. **(C)** Histological evaluation of glandular destruction in WT and KO mice was performed on tissue sections of submandibular glands with H&E staining. Bars, 100 µm. **(D)** Infiltrated lymphocytes in the SGs were assessed for histological scores. *n* = 11. **(E)** Anti-IgG immunofluorescent staining of SG. Bars, 50 µm. *n* = 3 or 4 per group. **(F and G)** FACS staining (left) and frequency quantification (right) of the $CXCR5^+PD1^+$ Tfh cells among $CD4^+Foxp3^-$ (F) and Fas^+GL7^+ GCB cells among $B220^+$ cells (G) in CLN of WT and KO mice immunized for ESS induction at 15 wk after first immunization. *n* = 7–9 per group. **(H and I)** After restimulation with PMA and ionomycin for 5 h, frequencies of IFN-γ- and IL-17–producing Th1 (H) and Th17 (I) cells among the $CD4^+$ T cells in the CLN of WT and KO mice were examined by flow cytometry analysis. *n* = 10–16 per group. **(J and K)** The serum IFN-γ (J) and IL-17 (K) levels were detected by ELISA. *n* = 5 or 7 per group. Data in D and F–I were pooled from two independent experiments. All experimental data were verified in at least two independent experiments. $Bcl6^{fl/fl}Cd4^{Cre}$ were KO, and $Bcl6^{fl/fl}$ littermates from the $Bcl6^{fl/fl}Cd4^{Cre}$ were used as control. Data shown are mean ± SEM; two-tailed *t* test; p-values in B were analyzed by two-way ANOVA; *, $P < 0.05$; **, $P < 0.01$; ***, $P < 0.001$; ****, $P < 0.0001$; n.s., no significance.

sponse, the mice were challenged using NP-KLH (1 mg/ml) emulsified in IFA after 30 d. dLN cells were stained with fluorescence-labeled antibodies and analyzed with a Fortessa instrument and FlowJo software. Intracellular staining was performed with kits from eBioscience. Sera from immunized mice were collected, and antigen-specific antibodies were measured using ELISA as described previously (Chung et al., 2011). In brief, serum samples were added in a threefold serial dilution onto plates precoated with 10 µg/ml NP_4-BSA (for high affinity) or NP_{29}-BSA (for global affinity), followed by HRP-conjugated antibodies.

Influenza virus infection

6-wk-old *Bcl6*$^{fl/fl}$*Foxp3Cre/Cre* mice were anesthetized and infected intranasally with 0.1 LD_{50} of PR8 influenza virus. Mice were monitored daily, and weight loss was recorded. Tfh and GC B cells from lung mediastinal lymph nodes were analyzed by flow cytometry. Sera were collected from virus-infected mice on day 9 after infection. Virus-specific antibodies were measured with ELISA as previously described (Liu et al., 2014). Briefly, serum samples were added in a threefold serial dilution onto plates precoated with heat-inactivated virus. Lung viral titers were monitored by examining influenza virus HA gene expression using real-time RT-PCR as previously described (Liu et al., 2014).

ESS model induction

The ESS mouse model was induced in 7–8-wk-old female mice by immunization with SG proteins as described before, with modifications (Lin et al., 2015). In brief, the bilateral SG from mice was collected for homogenization in PBS, and the supernatant was collected. The mice were immunized with SG proteins (5 mg/ml) emulsified in CFA (5 mg/ml) s.c. (200 µl each mouse) on the neck on day 0. On day 14, the booster injection was performed with a dose of 1.25 mg/ml SG proteins emulsified in IFA (Sigma-Aldrich). After the animals were anesthetized, saliva flow was collected for 10 min. Serum was obtained for SG-specific antibody analysis.

Histological examination and immunofluorescence microscopy

Tissues were excised from the mice, fixed in 4% paraformaldehyde, and prepared for sectioning with hematoxylin and eosin (H&E) staining. A widely used scoring system based on the size and degree of lymphoid organization of the infiltrates was adopted to assess the severity of tissue damage (Scardina et al., 2007). Immunohistochemical analysis was performed as previously described (Nurieva et al., 2009). Tissue blocks were sliced to ∼12 µm, air dried, and fixed with cold acetone. Tissue slides were stained with primary antibodies against biotinylated PNA (Vector Laboratories), and eFluor 450–conjugated rat anti-mouse/rat Foxp3 (clone FJK16S; eBioscience), followed by Streptavidin-APC (BD PharMingen). For IgG deposit detection, frozen sections were stained with FITC goat anti–mouse IgG F(ab′)2 (Thermo Fisher Scientific). Serum anti-dsDNA autoantibodies were detected as described (Vaeth et al., 2016) by coating ELISA plates (which were treated with poly-L-lysine solution; Sigma-Aldrich) with 2.5 µg/ml calf-thymus dsDNA (Sigma-Aldrich). The anti-dsDNA IgG standard was from Alpha Diagnostic. Anti-ANA antibodies were detected using an ELISA kit from Alpha Diagnostic. Anti-nRNP/Sm antibody analysis was done using a nRNP/Sm-coated plate from Euroimmun and detected with HRP-labeled Abs (SouthernBiotech).

Statistical analyses

Data were compared using a two-tailed unpaired Student's *t* test or two-way ANOVA (GraphPad software). Differences with p-values of <0.05 were considered significant: *, $P < 0.05$; **, P < 0,005; ***, $P < 0.001$; n.s, no significance.

Online supplemental material

Fig. S1 shows flow cytometry and immunofluorescence analysis of Tfr cells after KLH immunization, the effect of Tfr deficiency to Tfh, GC B, and memory B cells; LZ/DZ ratio by flow cytometry; ELISA data of the antigen-specific Abs production and affinity; and phenotype validation in the influenza infection model using littermate controls. Fig. S2 shows the effect of Tfr deficiency in the unmanipulated mice at ages 6–8 and 12 wk, autoantibody production in 30-wk-old mice, and H&E and FACS data of 30-wk-old mice using littermate controls. Fig. S3 shows the ESS model establishment; Tfh, Tfr, and GC B cell expression in the ESS model; and H&E analysis of the mice 5 wk after ESS induction using littermate controls.

ACKNOWLEDGMENTS

We thank A. Rudensky for *Foxp3*^{Cre} mice, S. Feske for sharing the protocol to detect serum anti-dsDNA antibody, the flow cytometry facility at the Institute for Immunology at Tsinghua University for help in cell sorting, and members of the Dong laboratory for technical support and assistance.

This work was supported in part by the National Natural Science Foundation of China (91642201 to C. Dong and 31600718 to W. Fu) and a Chinese Ministry of Science and Technology grant (2016YFC0906200 to C. Dong).

The authors declare no competing financial interests.

Author contributions: W. Fu designed, performed the experiments, and wrote the manuscript. X. Liu generated the *Bcl6*$^{fl/fl}$ mice. X. Lin and L. Lu contributed to the ESS model establishment and the pathology analysis. H. Feng and L. Sun performed experiments. S. Li, H. Chen, and H. Tang contributed to the influenza virus preparation and infection model establishment. W. Jin reviewed and edited the manuscript. C. Dong designed the research and edited the manuscript.

Submitted: 18 May 2017
Revised: 27 October 2017
Accepted: 18 December 2017

REFERENCES

Aloulou, M., E.J. Carr, M. Gador, A. Bignon, R.S. Liblau, N. Fazilleau, and M.A. Linterman. 2016. Follicular regulatory T cells can be specific for the immunizing antigen and derive from naive T cells. *Nat. Commun.* 7:10579. https://doi.org/10.1038/ncomms10579

Botta, D., M.J. Fuller, T.T. Marquez-Lago, H. Bachus, J.E. Bradley, A.S. Weinmann, A.J. Zajac, T.D. Randall, F.E. Lund, B. León, and A. Ballesteros-Tato. 2017. Dynamic regulation of T follicular regulatory cell responses by interleukin 2 during influenza infection. *Nat. Immunol.* 18:1249–1260. https://doi.org/10.1038/ni.3837

Chung, Y., S. Tanaka, F. Chu, R.I. Nurieva, G.J. Martinez, S. Rawal, Y.H. Wang, H. Lim, J.M. Reynolds, X.H. Zhou, et al. 2011. Follicular regulatory T cells expressing Foxp3 and Bcl-6 suppress germinal center reactions. *Nat. Med.* 17:983–988. https://doi.org/10.1038/nm.2426

Crotty, S. 2011. Follicular helper CD4 T cells (TFH). *Annu. Rev. Immunol.* 29:621–663. https://doi.org/10.1146/annurev-immunol-031210-101400

Crotty, S. 2014. T follicular helper cell differentiation, function, and roles in disease. *Immunity.* 41:529–542. https://doi.org/10.1016/j.immuni.2014.10.004

Gerner, M.Y., P. Torabi-Parizi, and R.N. Germain. 2015. Strategically localized dendritic cells promote rapid T cell responses to lymph-borne particulate antigens. *Immunity.* 42:172–185. https://doi.org/10.1016/j.immuni.2014.12.024

Gómez-Martín, D., M. Díaz-Zamudio, J. Romo-Tena, M.J. Ibarra-Sánchez, and J. Alcocer-Varela. 2011. Follicular helper T cells poise immune responses to the development of autoimmune pathology. *Autoimmun. Rev.* 10:325–330. https://doi.org/10.1016/j.autrev.2010.11.007

Jandl, C., S.M. Liu, P.F. Cañete, J. Warren, W.E. Hughes, A. Vogelzang, K. Webster, M.E. Craig, G. Uzel, A. Dent, et al. 2017. IL-21 restricts T follicular regulatory T cell proliferation through Bcl-6 mediated inhibition of responsiveness to IL-2. *Nat. Commun.* 8:14647. https://doi.org/10.1038/ncomms14647

Johnston, R.J., A.C. Poholek, D. DiToro, I. Yusuf, D. Eto, B. Barnett, A.L. Dent, J. Craft, and S. Crotty. 2009. Bcl6 and Blimp-1 are reciprocal and antagonistic regulators of T follicular helper cell differentiation. *Science.* 325:1006–1010. https://doi.org/10.1126/science.1175870

Kerfoot, S.M., G. Yaari, J.R. Patel, K.L. Johnson, D.G. Gonzalez, S.H. Kleinstein, and A.M. Haberman. 2011. Germinal center B cell and T follicular helper cell development initiates in the interfollicular zone. *Immunity.* 34:947–960. https://doi.org/10.1016/j.immuni.2011.03.024

Lin, X., K. Rui, J. Deng, J. Tian, X. Wang, S. Wang, K.H. Ko, Z. Jiao, V.S. Chan, C.S. Lau, et al. 2015. Th17 cells play a critical role in the development of experimental Sjögren's syndrome. *Ann. Rheum. Dis.* 74:1302–1310. https://doi.org/10.1136/annrheumdis-2013-204584

Linterman, M.A., W. Pierson, S.K. Lee, A. Kallies, S. Kawamoto, T.F. Rayner, M. Srivastava, D.P. Divekar, L. Beaton, J.J. Hogan, et al. 2011. Foxp3+ follicular regulatory T cells control the germinal center response. *Nat. Med.* 17:975–982. https://doi.org/10.1038/nm.2425

Liu, X., X. Yan, B. Zhong, R.I. Nurieva, A. Wang, X. Wang, N. Martin-Orozco, Y. Wang, S.H. Chang, E. Esplugues, et al. 2012. Bcl6 expression specifies the T follicular helper cell program in vivo. *J. Exp. Med.* 209:1841–1852. https://doi.org/10.1084/jem.20120219

Liu, X., X. Chen, B. Zhong, A. Wang, X. Wang, F. Chu, R.I. Nurieva, X. Yan, P. Chen, L.G. van der Flier, et al. 2014. Transcription factor achaete-scute homologue 2 initiates follicular T-helper-cell development. *Nature.* 507:513–518. https://doi.org/10.1038/nature12910

Liu, X., H. Lu, T. Chen, K.C. Nallaparaju, X. Yan, S. Tanaka, K. Ichiyama, X. Zhang, L. Zhang, X. Wen, et al. 2016. Genome-wide analysis identifies Bcl6-controlled regulatory networks during T follicular helper cell differentiation. *Cell Reports.* 14:1735–1747. https://doi.org/10.1016/j.celrep.2016.01.038

Liu, Z., M.Y. Gerner, N. Van Panhuys, A.G. Levine, A.Y. Rudensky, and R.N. Germain. 2015. Immune homeostasis enforced by co-localized effector and regulatory T cells. *Nature.* 528:225–230. https://doi.org/10.1038/nature16169

Lüthje, K., A. Kallies, Y. Shimohakamada, G.T. Belz, A. Light, D.M. Tarlinton, and S.L. Nutt. 2012. The development and fate of follicular helper T cells defined by an IL-21 reporter mouse. *Nat. Immunol.* 13:491–498. https://doi.org/10.1038/ni.2261

Miyazaki, M., K. Miyazaki, S. Chen, M. Itoi, M. Miller, L.F. Lu, N. Varki, A.N. Chang, D.H. Broide, and C. Murre. 2014. Id2 and Id3 maintain the regulatory T cell pool to suppress inflammatory disease. *Nat. Immunol.* 15:767–776. https://doi.org/10.1038/ni.2928

Nurieva, R.I., Y. Chung, G.J. Martinez, X.O. Yang, S. Tanaka, T.D. Matskevitch, Y.H. Wang, and C. Dong. 2009. Bcl6 mediates the development of T follicular helper cells. *Science.* 325:1001–1005. https://doi.org/10.1126/science.1176676

Reinhardt, R.L., H.E. Liang, and R.M. Locksley. 2009. Cytokine-secreting follicular T cells shape the antibody repertoire. *Nat. Immunol.* 10:385–393. https://doi.org/10.1038/ni.1715

Sage, P.T., L.M. Francisco, C.V. Carman, and A.H. Sharpe. 2013. The receptor PD-1 controls follicular regulatory T cells in the lymph nodes and blood. *Nat. Immunol.* 14:152–161. https://doi.org/10.1038/ni.2496

Sage, P.T., D. Alvarez, J. Godec, U.H. von Andrian, and A.H. Sharpe. 2014a. Circulating T follicular regulatory and helper cells have memory-like properties. *J. Clin. Invest.* 124:5191–5204. https://doi.org/10.1172/JCI76861

Sage, P.T., A.M. Paterson, S.B. Lovitch, and A.H. Sharpe. 2014b. The coinhibitory receptor CTLA-4 controls B cell responses by modulating T follicular helper, T follicular regulatory, and T regulatory cells. *Immunity.* 41:1026–1039. https://doi.org/10.1016/j.immuni.2014.12.005

Sage, P.T., C.L. Tan, G.J. Freeman, M. Haigis, and A.H. Sharpe. 2015. Defective TFH cell function and increased TFR cells contribute to defective antibody production in aging. *Cell Reports.* 12:163–171. https://doi.org/10.1016/j.celrep.2015.06.015

Sage, P.T., N. Ron-Harel, V.R. Juneja, D.R. Sen, S. Maleri, W. Sungnak, V.K. Kuchroo, W.N. Haining, N. Chevrier, M. Haigis, and A.H. Sharpe. 2016. Suppression by TFR cells leads to durable and selective inhibition of B cell effector function. *Nat. Immunol.* 17:1436–1446. https://doi.org/10.1038/ni.3578

Scardina, G.A., G. Spanó, F. Carini, M. Spicola, V. Valenza, P. Messina, and E. Maresi. 2007. Diagnostic evaluation of serial sections of labial salivary gland biopsies in Sjögren's syndrome. *Med. Oral Patol. Oral Cir. Bucal.* 12:E565–E568.

Snapper, C.M., and W.E. Paul. 1987. Interferon-gamma and B cell stimulatory factor-1 reciprocally regulate Ig isotype production. *Science.* 236:944–947. https://doi.org/10.1126/science.3107127

Takahashi, Y., H. Ohta, and T. Takemori. 2001. Fas is required for clonal selection in germinal centers and the subsequent establishment of the memory B cell repertoire. *Immunity.* 14:181–192. https://doi.org/10.1016/S1074-7613(01)00100-5

Vaeth, M., G. Müller, D. Stauss, L. Dietz, S. Klein-Hessling, E. Serfling, M. Lipp, I. Berberich, and F. Berberich-Siebelt. 2014. Follicular regulatory T cells control humoral autoimmunity via NFAT2-regulated CXCR5 expression. *J. Exp. Med.* 211:545–561. https://doi.org/10.1084/jem.20130604

Vaeth, M., M. Eckstein, P.J. Shaw, L. Kozhaya, J. Yang, F. Berberich-Siebelt, R. Clancy, D. Unutmaz, and S. Feske. 2016. Store-operated Ca(2+) entry in follicular T cells controls humoral immune responses and autoimmunity. *Immunity.* 44:1350–1364. https://doi.org/10.1016/j.immuni.2016.04.013

Victora, G.D., T.A. Schwickert, D.R. Fooksman, A.O. Kamphorst, M. Meyer-Hermann, M.L. Dustin, and M.C. Nussenzweig. 2010. Germinal center dynamics revealed by multiphoton microscopy with a photoactivatable fluorescent reporter. *Cell.* 143:592–605. https://doi.org/10.1016/j.cell.2010.10.032

Victora, G.D., D. Dominguez-Sola, A.B. Holmes, S. Deroubaix, R. Dalla-Favera, and M.C. Nussenzweig. 2012. Identification of human germinal center light and dark zone cells and their relationship to human B-cell

lymphomas. *Blood*. 120:2240–2248. https://doi.org/10.1182/blood-2012-03-415380

Vinuesa, C.G., I. Sanz, and M.C. Cook. 2009. Dysregulation of germinal centres in autoimmune disease. *Nat. Rev. Immunol.* 9:845–857. https://doi.org/10.1038/nri2637

Wang, Y., J. Shi, J. Yan, Z. Xiao, X. Hou, P. Lu, S. Hou, T. Mao, W. Liu, Y. Ma, et al. 2017. Germinal-center development of memory B cells driven by IL-9 from follicular helper T cells. *Nat. Immunol.* 18:921–930. https://doi.org/10.1038/ni.3788

Wing, J.B., W. Ise, T. Kurosaki, and S. Sakaguchi. 2014. Regulatory T cells control antigen-specific expansion of Tfh cell number and humoral immune responses via the coreceptor CTLA-4. *Immunity.* 41:1013–1025. https://doi.org/10.1016/j.immuni.2014.12.006

Wing, J.B., Y. Kitagawa, M. Locci, H. Hume, C. Tay, T. Morita, Y. Kidani, K. Matsuda, T. Inoue, T. Kurosaki, et al. 2017. A distinct subpopulation of CD25- T-follicular regulatory cells localizes in the germinal centers. *Proc. Natl. Acad. Sci. USA.* 114:E6400–E6409. https://doi.org/10.1073/pnas.1705551114

Wollenberg, I., A. Agua-Doce, A. Hernández, C. Almeida, V.G. Oliveira, J. Faro, and L. Graca. 2011. Regulation of the germinal center reaction by Foxp3+ follicular regulatory T cells. *J. Immunol.* 187:4553–4560. https://doi.org/10.4049/jimmunol.1101328

Yu, D., S. Rao, L.M. Tsai, S.K. Lee, Y. He, E.L. Sutcliffe, M. Srivastava, M. Linterman, L. Zheng, N. Simpson, et al. 2009. The transcriptional repressor Bcl-6 directs T follicular helper cell lineage commitment. *Immunity.* 31:457–468. https://doi.org/10.1016/j.immuni.2009.07.002

Zotos, D., J.M. Coquet, Y. Zhang, A. Light, K. D'Costa, A. Kallies, L.M. Corcoran, D.I. Godfrey, K.M. Toellner, M.J. Smyth, et al. 2010. IL-21 regulates germinal center B cell differentiation and proliferation through a B cell-intrinsic mechanism. *J. Exp. Med.* 207:365–378. https://doi.org/10.1084/jem.20091777